Electronic Supplementary Material (ESI) for Materials Chemistry Frontiers.

Co-assembly of sugar-based amphiphilic block polymers to achieve nanoparticles with tunable morphology, size, surface charge, and acid-responsive behavior

Yen-Nan Lin,[a,b] Lu Su,[a] Justin Smolen,[a] Richen Li,[a] Yue Song,[a] Hai Wang,[a] Mei Dong,[a] and Karen L. Wooley[a]

[a] Departments of Chemistry, Chemical Engineering, Materials Science & Engineering, and the Laboratory for Synthetic-Biologic Interactions, Texas A&M University, College Station, Texas 77842, USA

[b] College of Medicine, Texas A&M University, Bryan, Texas 77807, USA

Table of Contents

Instrumentation

^{1}H NMR and ^{13}C NMR spectra were recorded on a Varian 500 spectrometer (Varian, Inc., Palo Alto, CA) interfaced to a UNIX computer using VNMR-J software. All NMR experiments were performed at ambient temperature. Chemical shifts were referenced to the solvent residual signals. All ^{1}H NMR chemical shifts are reported in parts per million (ppm) downfield of tetramethylsilane and relative to the signals for residual $CHCl_3$ (7.26 ppm). All ^{13}C NMR spectra are reported in ppm relative to $CDCl_3$ (77.23 ppm) and were obtained with ^{1}H decoupling.

Fourier transform infrared (FTIR) spectra were recorded on an IR Prestige 21 system equipped with a diamond attenuated total reflection (ATR) lens (Shimadzu Corp., Japan) and analyzed using IRsolution v. 1.40 software.

Size exclusion chromatography (SEC) eluting with tetrahydrofuran (THF) was performed on a Waters Chromatography, Inc. (Milford, MA) system equipped with an isocratic pump (model 1515), a differential refractometer (model 2414), and column set comprised of a PLgel 5 µm guard column (50 × 7.5 mm), a PLgel 5 µm Mixed C column (300 × 7.5 mm, Agilent Technologies) and two Styragel® columns (500 Å and 104 Å, 300 × 7.5 mm, Waters Chromatography, Inc.). The system was operated at 40 °C with a flow rate of 1 mL/min. Data were analyzed using Breeze software from Waters Chromatography, Inc. (Milford, MA). Molar masses were determined relative to polystyrene standards (580–3,250,000 Da) purchased from Polymer Laboratories, Inc. (Amherst, MA). Polymer solutions were prepared at a concentration of *ca.* 3 mg/mL with 0.05 vol% toluene as the flow rate marker; an injection volume of 200 µL was used.

Thermogravimetric analysis (TGA) was performed under Ar atmosphere using a Mettler-Toledo TGA2/1100/464, with a heating rate of 10 °C/min, from 25 to 500 °C. Data were analyzed using Mettler-Toledo STAR^{e} v. 15.00a software.

Glass transition (T_g) and melting (T_m) temperatures were measured by differential scanning calorimetry (DSC) on a Mettler-Toledo DSC3/700/1190 (Mettler-Toledo, Inc., Columbus, OH) under $N_{2(g)}$. The T_g was taken as the midpoint of the inflection tangent of the second heating scan. The T_m was taken as the maximum of the endothermic peak of the second heating scan. Measurements were performed with a heating rate of 10 °C/min and the data were analyzed using Mettler-Toledo STAR^{e} v. 15.00a software.

Dynamic light scattering (DLS) measurements were conducted using a Delsa Nano C instrument (Beckman Coulter, Inc., Fullerton, CA) equipped with a laser diode operating at 658 nm. Scattered light was detected at 165° and analyzed using a log correlator over 70 accumulations for a 0.5 mL of sample in a glass size cell (capacity = 0.9 mL). The photomultiplier aperture and attenuator were adjusted automatically to obtain a photon count rate of *ca.* 10 kcps. The particle size distribution and distribution averages were calculated using CONTIN particle size distribution analysis routines in Delsa Nano 2.31 software. The average diameter of the particles is reported as the intensity-, volume- and number-average particle diameter from 70 accumulations. All measurements were repeated 10 times.

The zeta potentials of the nanoparticles were determined by a Delsa Nano C particle analyzer (Beckman Coulter Inc., Fullerton, CA) equipped with a 30 mW dual laser diode at 658 nm. The zeta potential of the particles in suspension was obtained by measuring the electrophoretic mobility of the charged particles. Scattered light was detected at a 30° angle at 25 °C. The zeta potential was measured at five regions in the flow cell and a weighted mean was calculated. These five measurements were used to correct for electroosmotic flow induced in the cell due to the surface charge of the cell wall. The zeta potential is reported as the average and standard deviation of three measurements.

Transmission electron microscopy (TEM) images were collected on a JEOL 1200EX operated at 100 kV, and micrographs were recorded using a SIA-15C CCD camera. Samples for TEM were prepared as follows: 20 µL of aqueous polymer solution (0.5 mg/mL) was deposited onto a carbon-coated copper grid, and after 1 min, excess solution was quickly wicked away by a piece of filter paper. The samples were then negatively stained with a 1 wt% phosphotungstic acid (PTA) aqueous solution (20 µL). After 30 s, excess stain solution was quickly wicked away by a piece of filter paper and the samples were left to dry under ambient conditions prior to imaging.

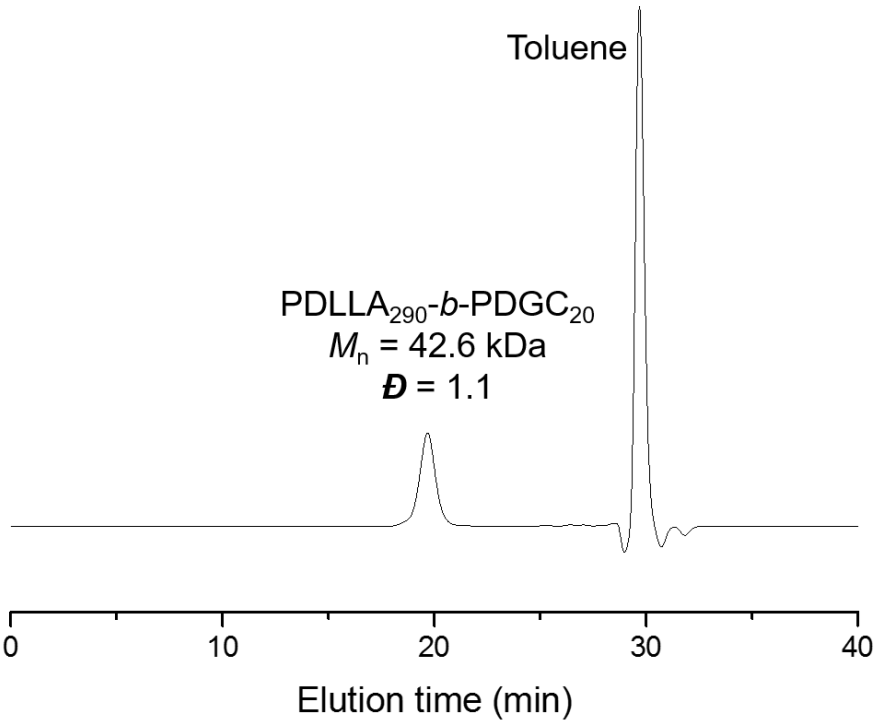

Figure S1. SEC trace of $PDLLA_{290}$-*b*-$PDGC_{20}$ in THF.

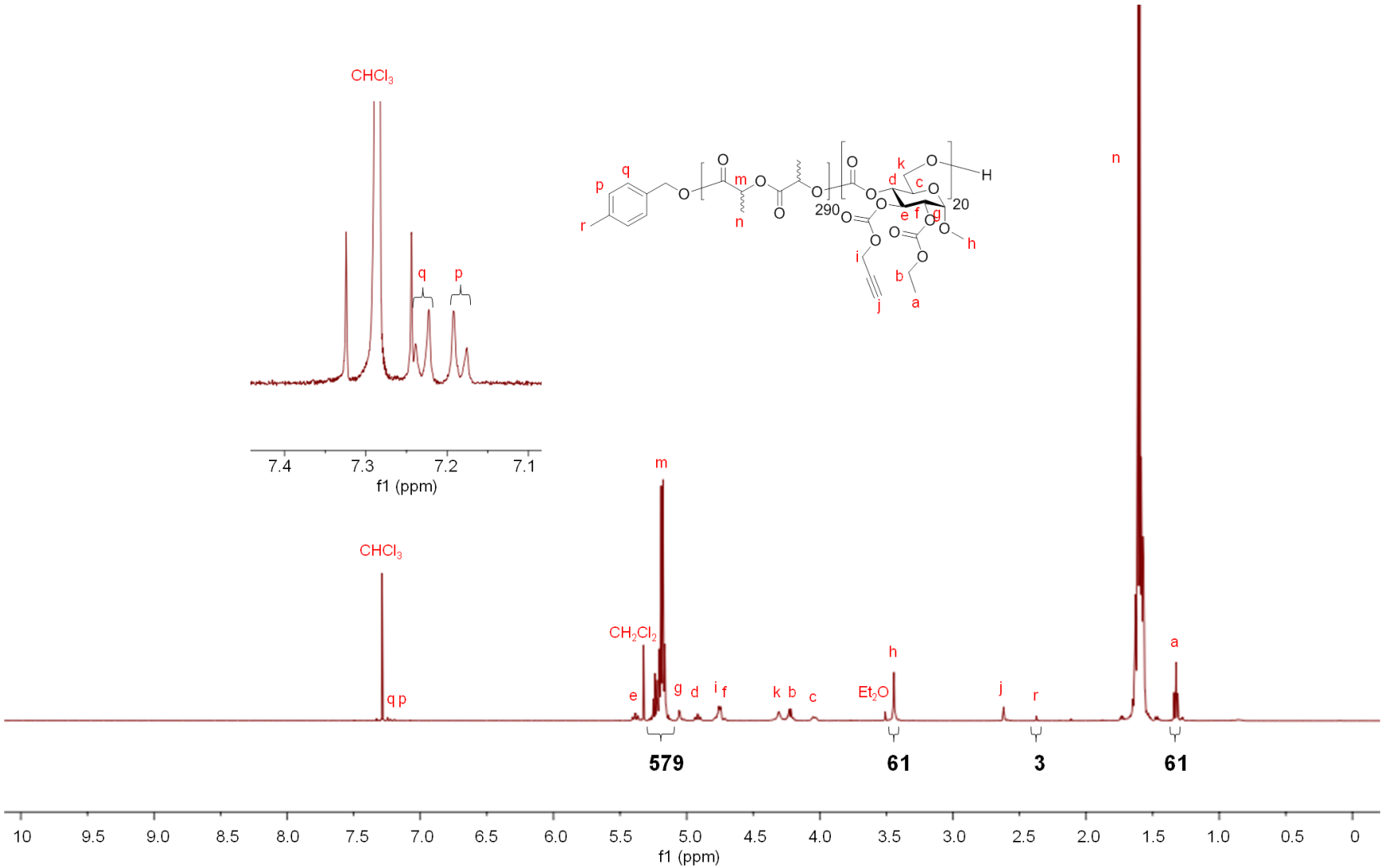

Figure S2. ^{1}H NMR spectrum (500 MHz) of PDLLA$_{290}$-*b*-PDGC$_{20}$ in $CDCl_3$, with the inset expanding the region to show the resonance signals for the aromatic protons of the α-chain end.

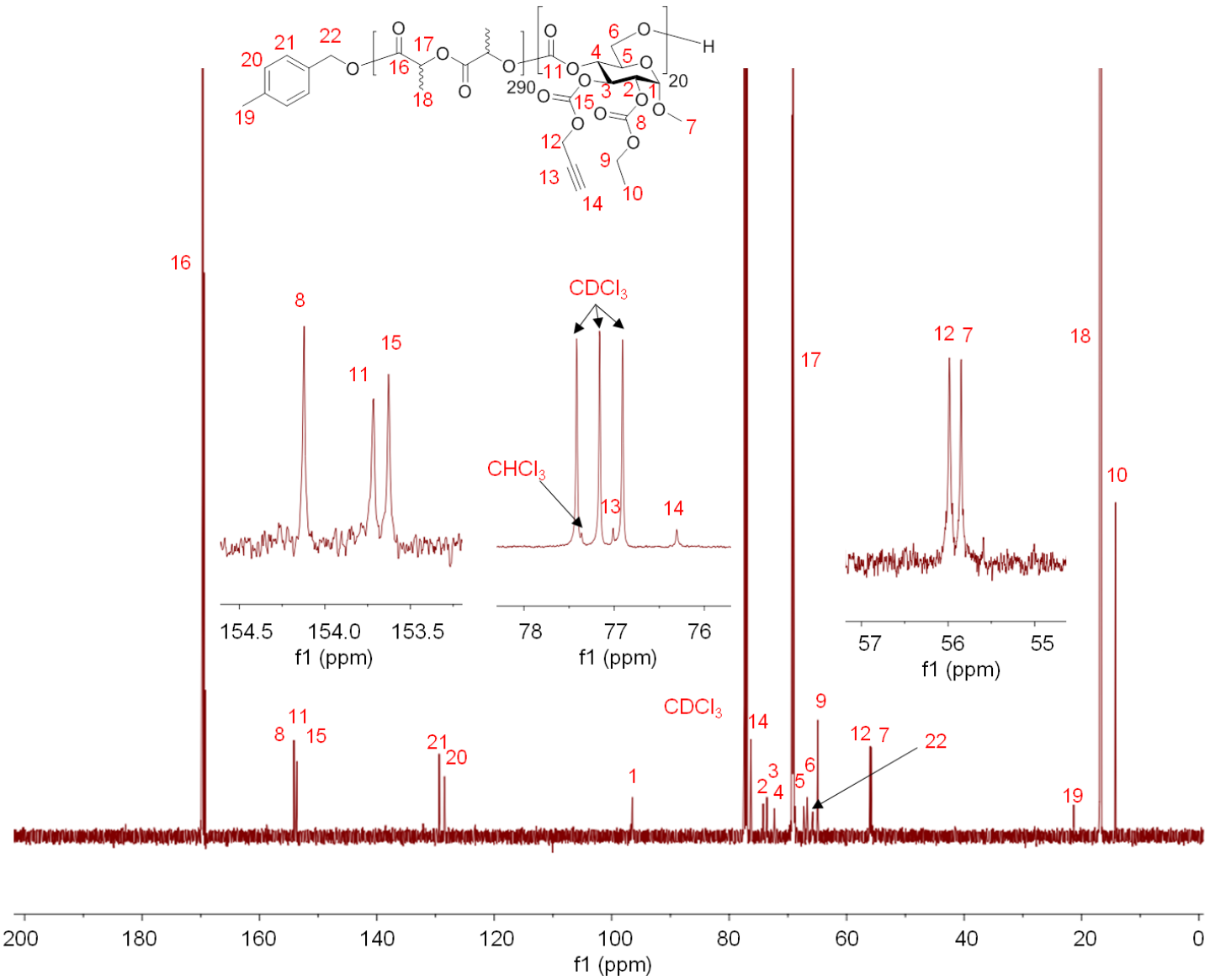

Figure S3. ^{13}C NMR spectrum (126 MHz) of $PDLLA_{290}$-*b*-$PDGC_{20}$ in $CDCl_3$.

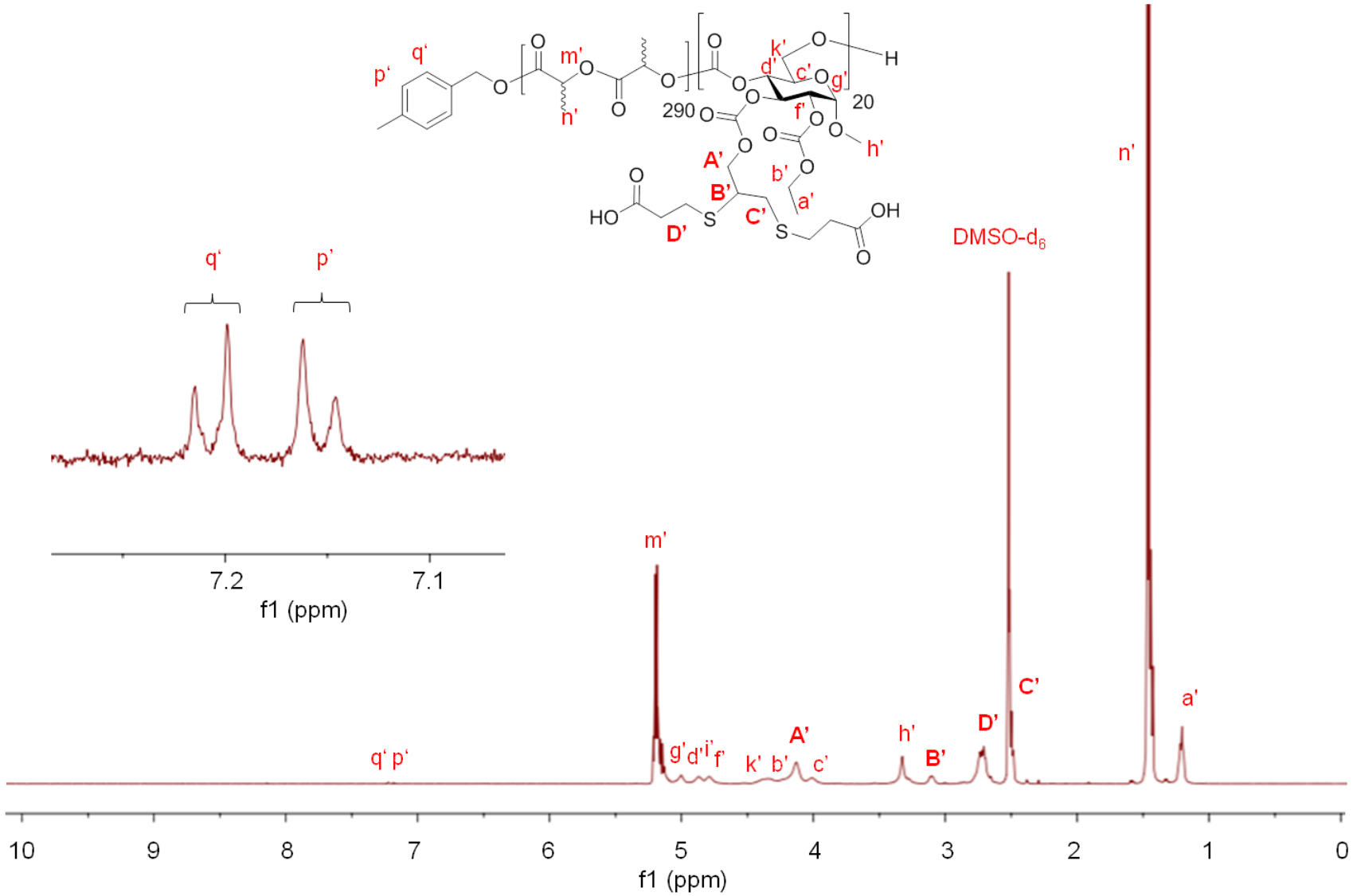

Figure S4. ^{1}H NMR spectrum (500 MHz) of PDLLA$_{290}$-*b*-PDGC(COOH)$_{20}$ in DMSO-d_6, with the inset expanding the region to show the resonance signals for the aromatic protons of the α-chain end.

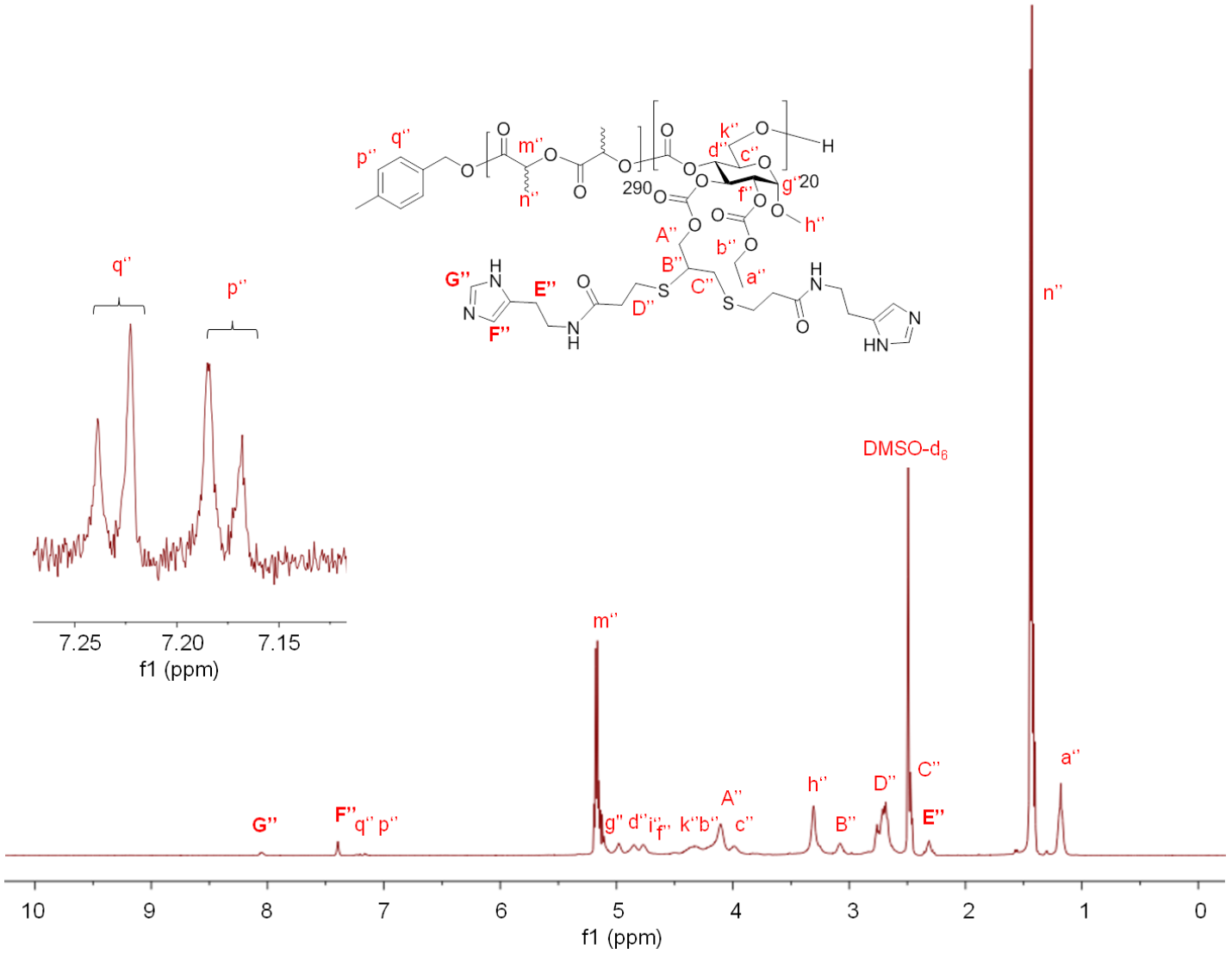

Figure S5. ^{1}H NMR spectrum (500 MHz) of PDLLA$_{290}$-*b*-PDGC(His)$_{20}$ in DMSO-d_6, with the inset expanding the region to show the resonance signals for the aromatic protons of the α-chain end.

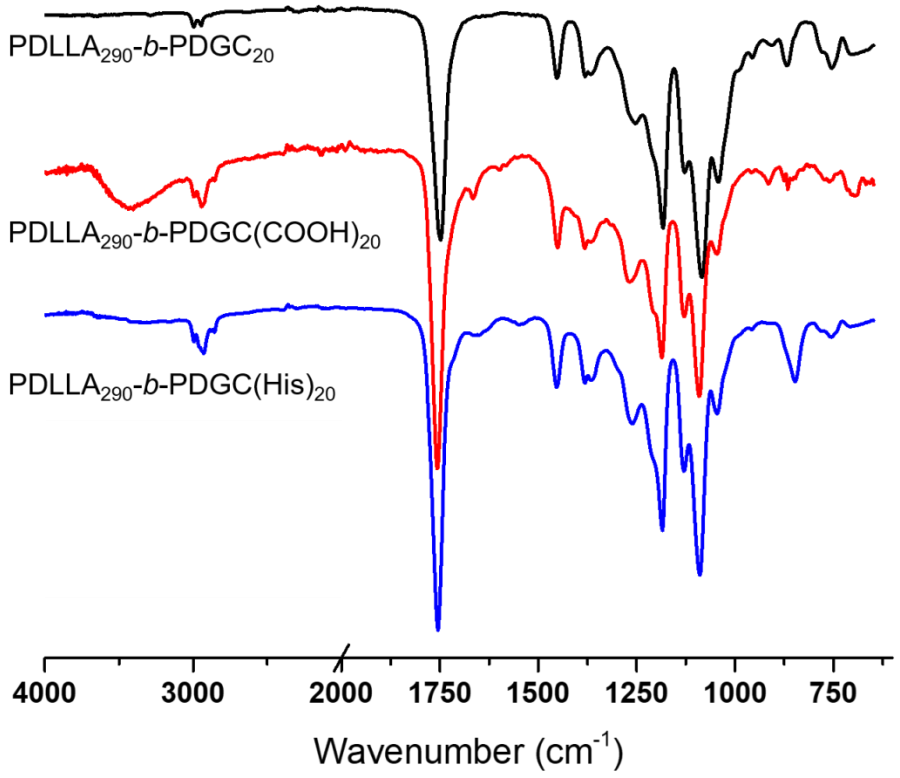

Figure S6. FT-IR spectra of $PDLLA_{290}$-*b*-$PDGC_{20}$, $PDLLA_{290}$-*b*-$PDGC(COOH)_{20}$, and $PDLLA_{290}$-*b*-$PDGC(His)_{20}$.

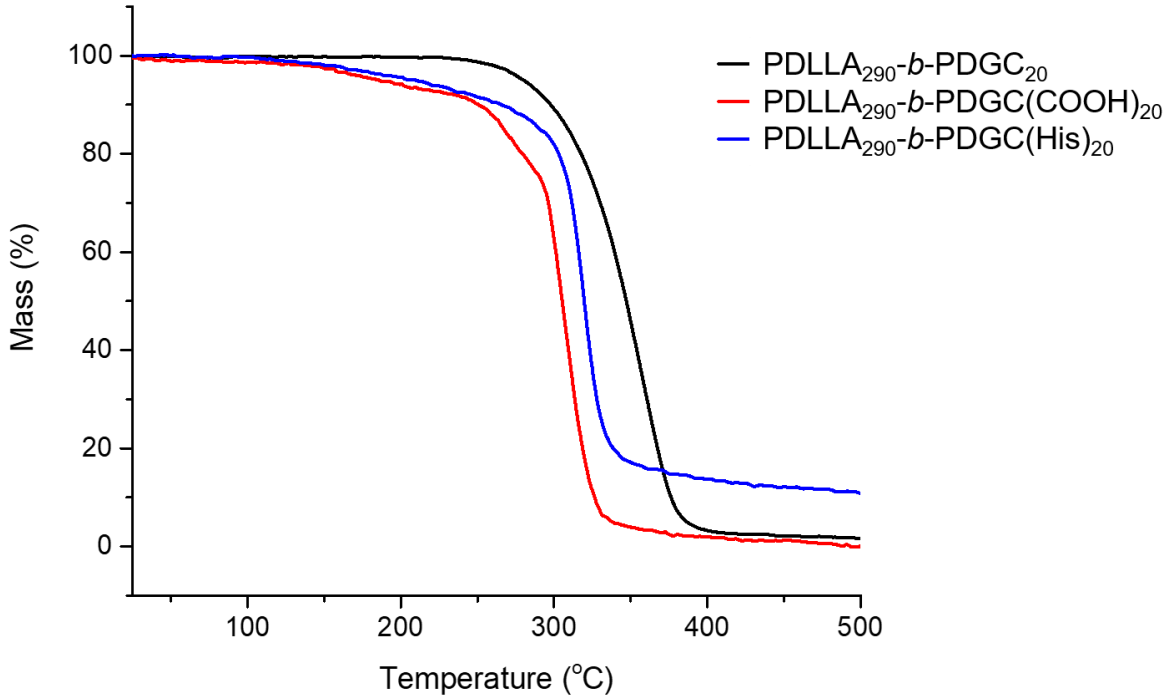

Figure S7. TGA traces of $PDLLA_{290}$-*b*-$PDGC_{20}$, $PDLLA_{290}$-*b*-$PDGC(COOH)_{20}$, and $PDLLA_{290}$-*b*-$PDGC(His)_{20}$.

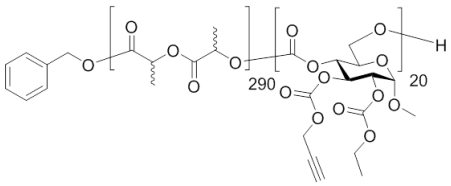

PDLLA$_{290}$-*b*-PDGC$_{20}$

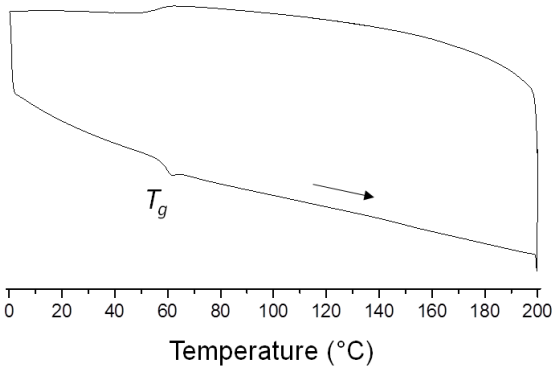

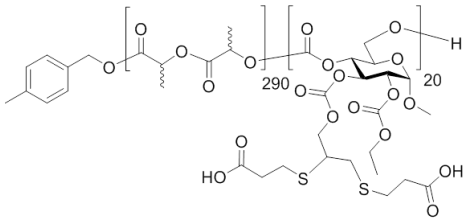

PDLLA$_{290}$-*b*-PDGC(COOH)$_{20}$

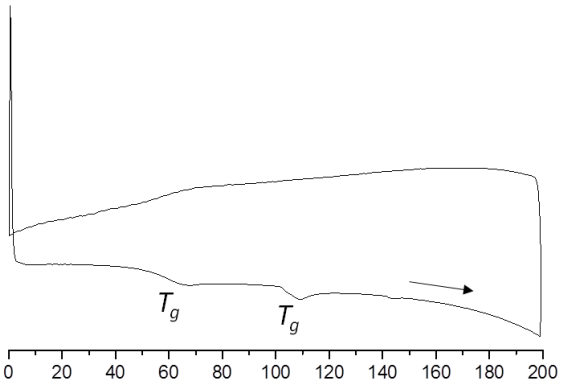

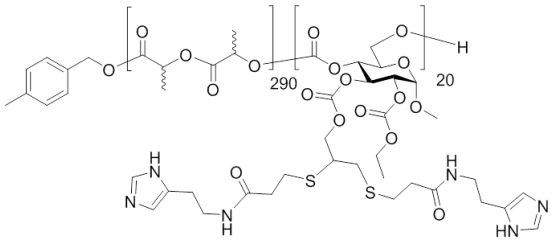

PDLLA$_{290}$-*b*-PDGC(His)$_{20}$

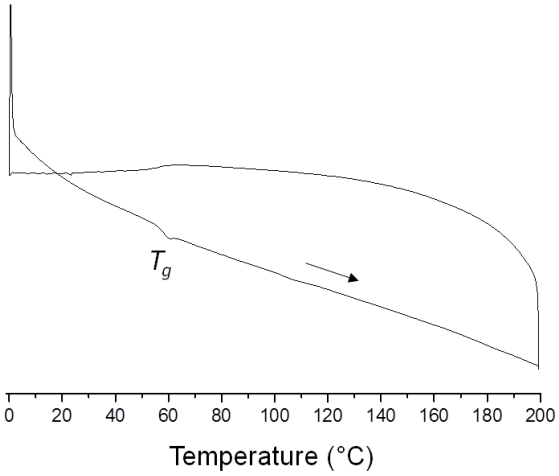

Figure S8. DSC curves for PDLLA$_{290}$-*b*-PDGC$_{20}$, PDLLA$_{290}$-*b*-PDGC(COOH)$_{20}$, and PDLLA$_{290}$-*b*-PDGC(His)$_{20}$. Glass transitions (T_g) are labeled on the thermograms. Arrows indicate the direction of temperature ramping.

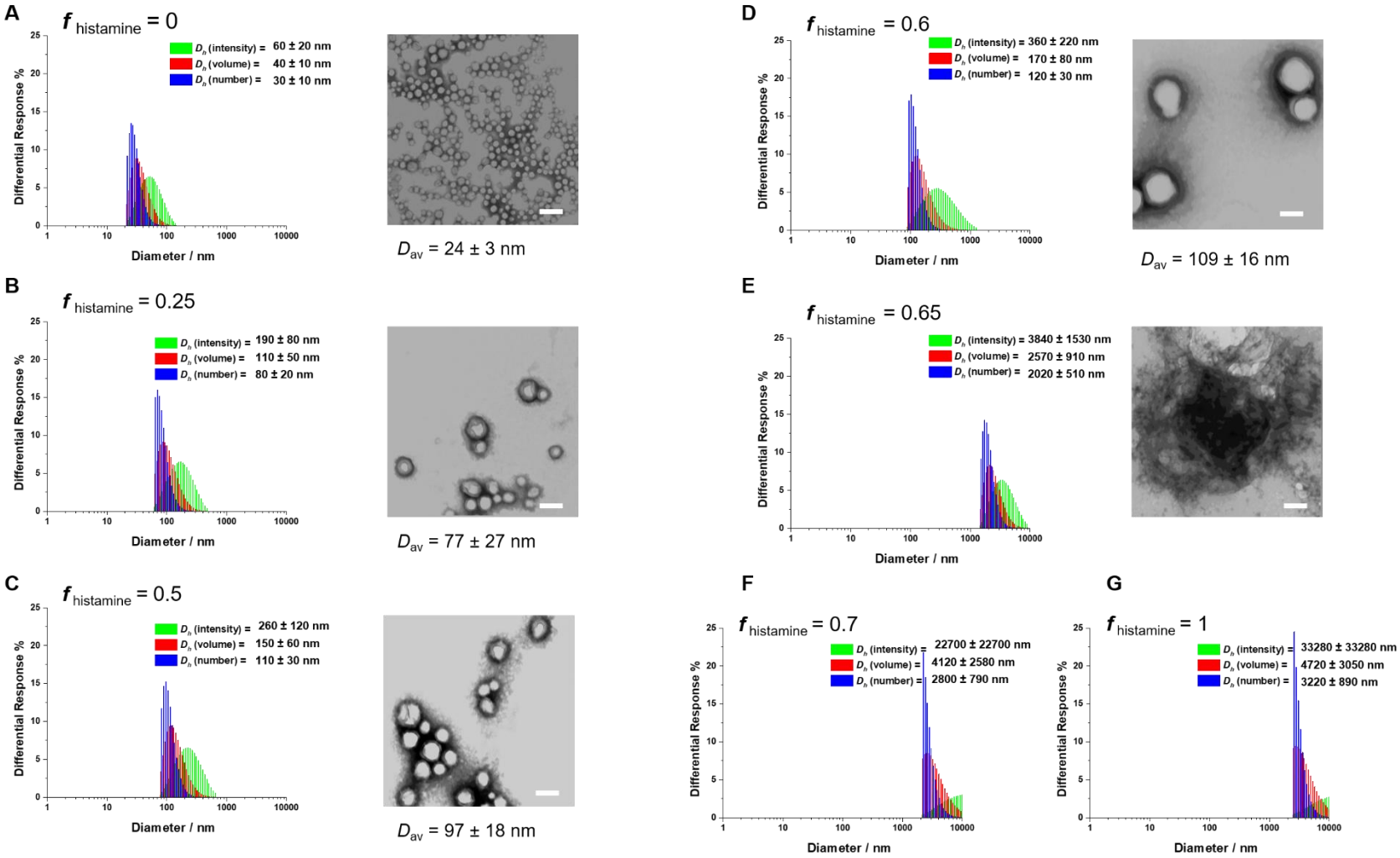

Figure S9. Dynamic light scattering (DLS) and transmission electron microscopy (TEM) of nanoparticles prepared by co-assembly of PDLLA$_{290}$-*b*-PDGC(COOH)$_{20}$ and PDLLA$_{290}$-*b*-PDGC(His)$_{20}$ in nanopure water at different PDLLA$_{290}$-*b*-PDGC(His)$_{20}$ contents, $f_{\text{histamine}}$ = (A) 0, (B) 0.25, (C) 0.5, (D) 0.6, (E) 0.65, (F) 0.7, (G) 1.0. TEM samples were negatively stained by 1 wt % phosphotungstic acid aqueous solution. The scale bars in the TEM images represent 100 nm. Visible precipitates were observed in samples with high $f_{\text{histamine}}$ (*i.e.*, E-G).

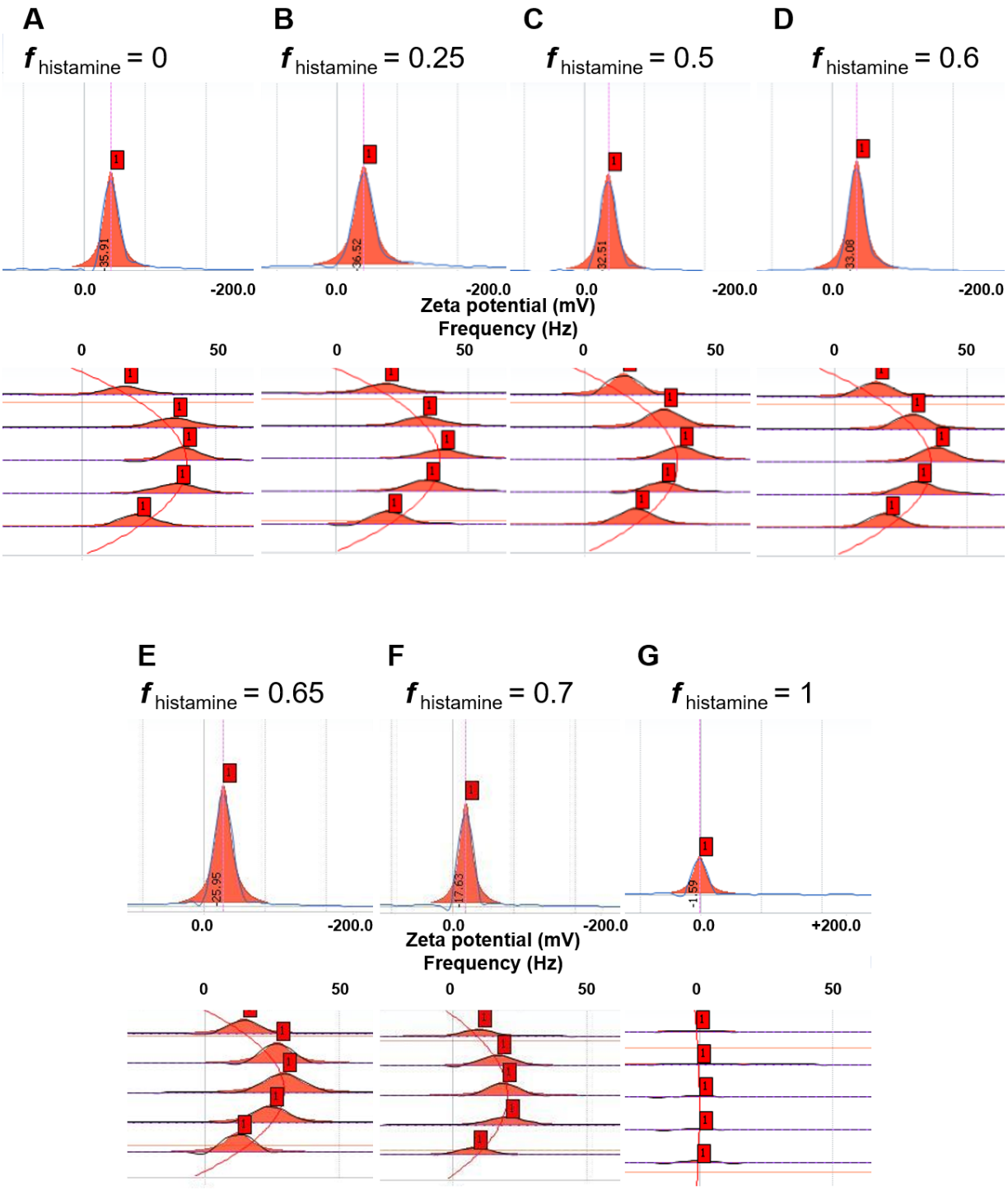

Figure S10. Zeta potential characterization of the nanoparticles in nanopure water prepared by co-assembly of PDLLA$_{290}$-*b*-PDGC(COOH)$_{20}$ and PDLLA$_{290}$-*b*-PDGC(His)$_{20}$ with $f_{\text{histamine}}$ = (A) 0, (B) 0.25, (C) 0.5, (D) 0.6, (E) 0.65, (F) 0.7, and (G) 1. Zeta potential Lorentzian peak (upper) and top view of frequency distribution (lower) as a function of position across the cell during the electrophoretic light scattering measurement.

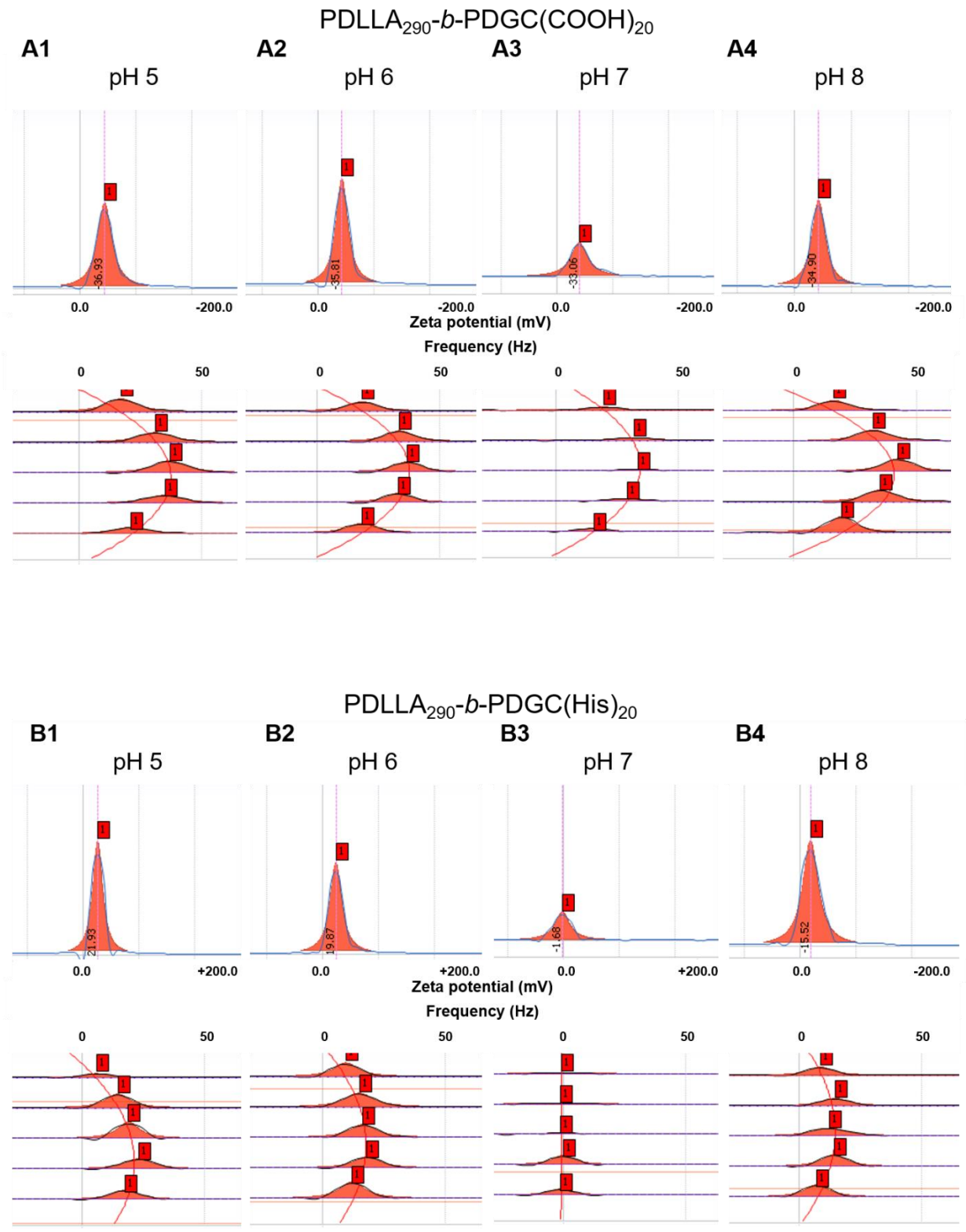

Figure S11. Zeta potential characterization of the nanoparticles prepared by self-assembly of (A) $PDLLA_{290}$-*b*-$PDGC(COOH)_{20}$ and (B) $PDLLA_{290}$-*b*-$PDGC(His)_{20}$ in MOPS buffer (20 mM) as a function of pH. Zeta potential Lorentzian peak (upper) and frequency distribution as a function of position across the cell during the electrophoretic light scattering measurement (lower).

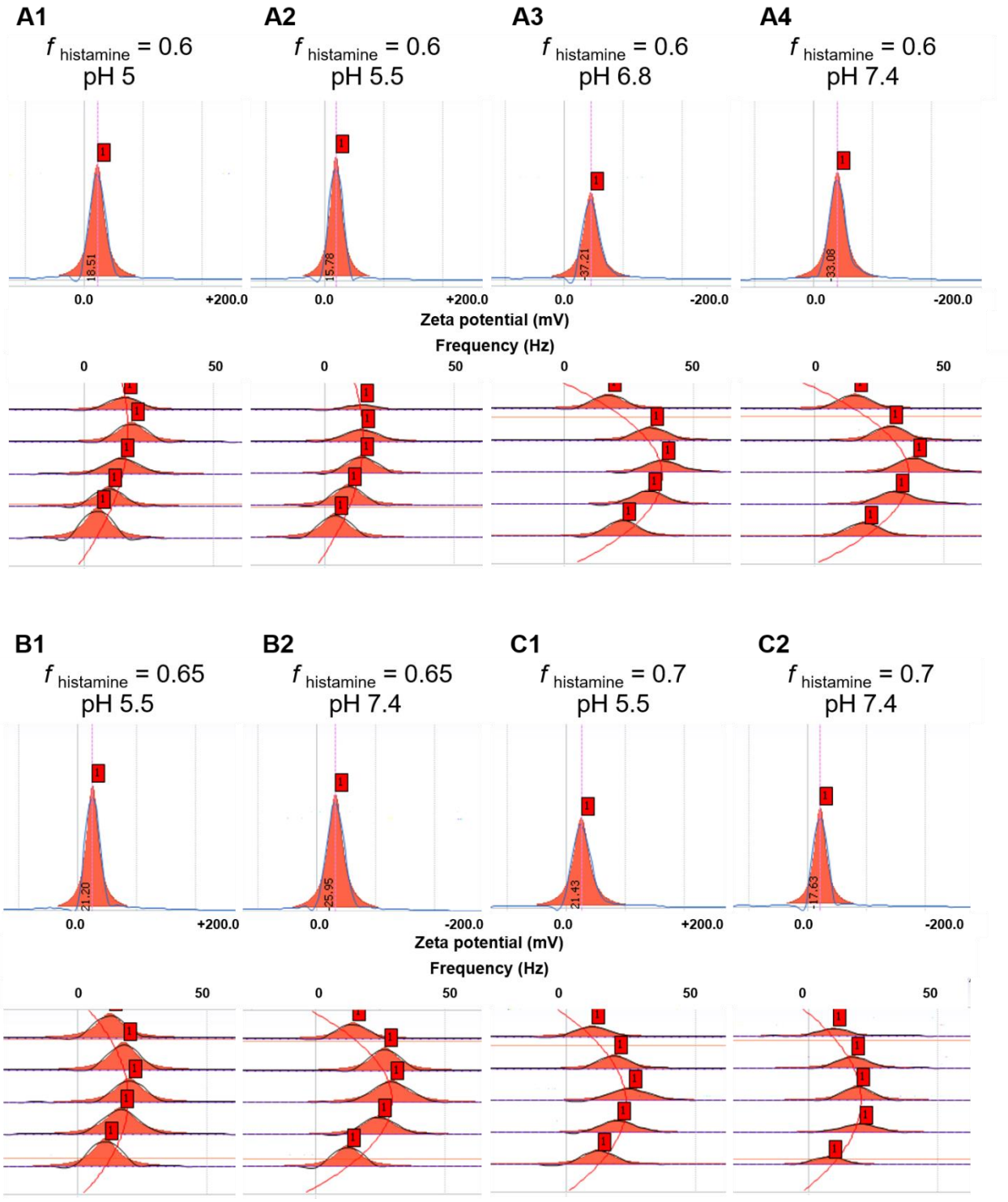

Figure S12. Zeta potential characterization of the nanoparticles prepared by co-assembly of PDLLA$_{290}$-*b*-PDGC(COOH)$_{20}$ and PDLLA$_{290}$-*b*-PDGC(His)$_{20}$ with $f_{\text{histamine}}$ = (A) 0.6, (B) 0.65, and (C) 0.7 in MOPS buffer (20 mM) as a function of pH. Zeta potential Lorentzian peak (upper) and top view of frequency distribution (lower) across the cell during electrophoretic light scattering measurement.

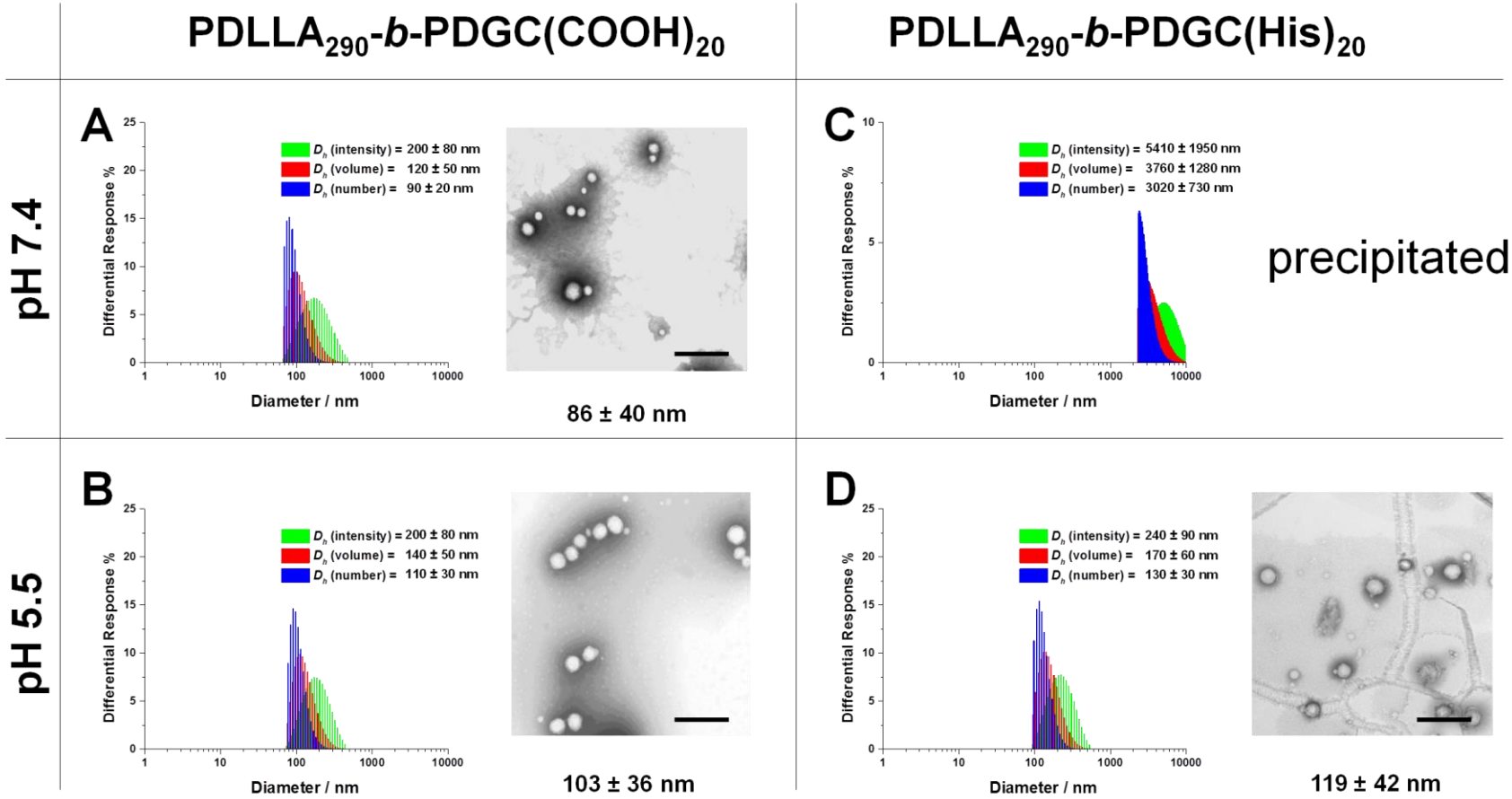

Figure S13. DLS and TEM of nanoparticles prepared by self-assembly of PDLLA$_{290}$-*b*-PDGC(COOH)$_{20}$ and PDLLA$_{290}$-*b*-PDGC(His)$_{20}$ in MOPS buffer (20 mM) at pH 5.5 and 7.4. TEM samples were negatively stained by 1 wt % phosphotungstic acid aqueous solution. The scale bars in the TEM images represent 500 nm. PDLLA$_{290}$-*b*-PDGC(His)$_{20}$ precipitated during assembly at pH 7.4.